JCTC Journal of Chemical Theory and Computation

Article

pubs.acs.org/JCTC

Simulation Study of the Structure and Phase Behavior of Ceramide Bilayers and the Role of Lipid Headgroup Chemistry

Shan Guo,[†] Timothy C. Moore,[†] Christopher R. Iacovella,[†] L. Anderson Strickland,[†] and Clare McCabe*[,†,‡]

[†]Department of Chemical and Biomolecular Engineering, Vanderbilt University, Nashville, Tennessee 37235, United States

[‡]Department of Chemistry, Vanderbilt University, Nashville, Tennessee 37235, United States

Supporting Information

ABSTRACT: Ceramides are known to be a key component of the stratum corneum, the outermost protective layer of the skin that controls barrier function. In this work, molecular dynamics simulations are used to examine the behavior of ceramide bilayers, focusing on nonhydroxy sphingosine (NS) and nonhydroxy phytosphingosine (NP) ceramides. Here, we propose a modified version of the CHARMM force field for ceramide simulation, which is directly compared to the more commonly used GROMOS-based force field of Berger (*Biophys. J.* **1997**, *72*, 2002−2013); while both force fields are shown to closely match experiment from a structural standpoint at the physiological temperature of skin, the modified CHARMM force field is better able to capture the thermotropic phase transitions observed in experiment. The role of ceramide chemistry and its impact on structural ordering is examined by comparing ceramide NS to NP, using the validated CHARMM-based force field. These simulations demonstrate that changing from ceramide NS to NP results in changes to the orientation of the OH groups in the lipid headgroups. The arrangement of OH groups perpendicular to the bilayer normal for ceramide NP, versus parallel for NS, results in the formation of a distinct hydrogen bonding network, which is ultimately responsible for shifting the gel-to-liquid phase transition to higher temperature, in direct agreement with experiment.

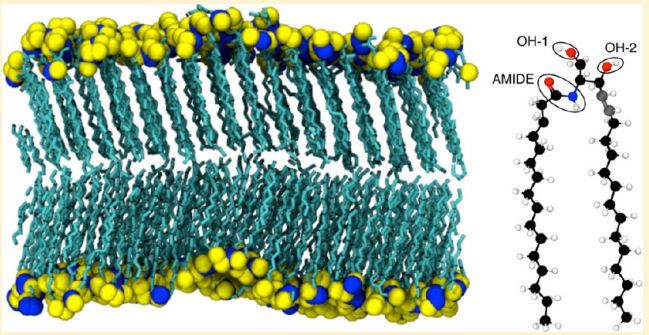

I. INTRODUCTION

The ability of the skin to regulate bodily functions and act as an effective barrier to chemical penetrants is controlled by the thin, outermost layer, known as the stratum corneum. The stratum corneum consists of dead, impenetrable skin cells (corneocytes) that are surrounded by a rich lipid matrix arranged in a brick-and-mortar-like configuration.[1] While the lipids of the stratum corneum are known to be predominantly composed of ceramides (CERs), cholesterol, and free fatty acids, the molecular level organization of the skin lipids and their role in maintaining the barrier function of the skin is not well understood.[2] It is, however, known that CERs play a crucial role in maintaining the physiological function of the stratum corneum[3] as a number of skin diseases[1,4] are known to be related to reduced CER levels in this layer.

Experimentally, 12 distinct CERs have been observed in the stratum corneum of human skin.[1,2,5−7] CERs are a class of double-tailed lipids consisting of hydrophobic acyl and sphingosine tails joined together by a hydrophilic headgroup. Based on the functional group attached to the sphingosine tail, CERs can be classified into sphingosines (S), phytosphingosines (P), and hydroxysphingosines (H). Sphingosines have an alkene bond in the sphinogsine tail; phytosphingosines have the alkene group replaced by a hydroxyl group; and hydroxysphingosines have a α-hydroxyl group connected to the alkene bond in the corresponding tail. The structures of the sphingosine and phytosphingosine CERs studied in this work are shown in figure 1. CERs can be further classified as either nonhydroxy (N) or α-hydroxy (A) CERs based on whether a hydroxyl group is attached to the carbon beside the carbonyl bond of the fatty acid tail. The subtle differences in molecular structure have been shown to influence phase transition temperatures and other characteristic properties of CER based bilayers.[7−13] Furthermore, while the length of the sphingoid tail is fairly constant at 16 carbons, the fatty acid tail exhibits considerable polydispersity in length; in human stratum corneum, the fatty acid tails range from 24 to 34 carbons,[2,3,5] resulting in considerable asymmetry between the lengths of the two tails.

The diversity of CERs that are found in the stratum corneum makes the investigation of their structure and behavior challenging. As a result, many experiments have focused on establishing the core behavior of CER-based systems by studying simplified "model" systems, e.g., bilayers composed of a single CER component or simple, well-defined mixtures. However, although these experimental investigations of lipid composition and organization are clearly critical, they can only

Received: May 24, 2013
Published: September 6, 2013

   dx.doi.org/10.1021/ct400431e | *J. Chem. Theory Comput.* 2013, 9, 5116−5126

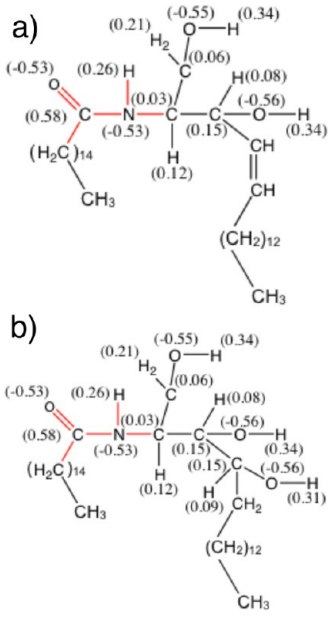

Figure 1. Molecular structure of (a) CER NS C_{16}, which belongs to the nonhydroxy sphingosine class of ceramides, and (b) CER NP C_{16}, a nonhydroxy phytosphingosine. The notation C_{16} is used to indicate the length of the CER acyl chain. The red in the figure indicates the bonded interactions of the CER molecule for which CHARMM parameters are proposed in this work. Numerical label in parentheses represents partial charges determined from *ab initio* calculations.

infer lipid structure and organization from consistency with analyses by several methods and molecular simulation could be used to elucidate the molecular level structure.[14−19]

While molecular simulation has been used extensively to study phospholipid bilayers and has provided a wealth of structural information,[20−22] in comparison, far less is known about the atomic level structure and interactions of bilayers involving CERs. This is, in part, related to the fact that neither GROMOS nor CHARMM—two of the most commonly used force fields for biological simulations—have been optimized specifically for CERs. Recent efforts have been made to adapt these force fields for CERs[23−25] by combining them with other force field parameter sets to handle missing interactions; however, these adapted parameters have not been extensively validated against experiment or compared. Of the limited simulation studies on CER bilayers reported in the literature, only CER NS has been considered.[24−31] In the first such study, Pandit and Scott[25] performed 20 ns simulations of a preassembled bilayer of CER NS C_{16} (where C_{16} indicates the number of carbons in the CER acyl chain) at ∼368 K using an adapted version of a force field developed by Chiu et al.[32] for sphingomyelin (SM); SM is similar to CER but has a large polar phosphorylcholine headgroup in place of the central hydroxyl group. From these relatively short simulations, it was found that intermolecular hydrogen bonding in CER NS was significantly altered as compared to that seen in a C_{18} SM bilayer and the absence of a large polar headgroup in CER NS significantly reduced the ordering of the water molecules at the lipid/water interface. Subsequently, Imai et al.[24] studied the residence time of water on the surface of preassembled CER NS bilayers using a fully atomistic model based on the CHARMM force field, finding that SM bilayers were capable of retaining water molecules longer than CER bilayers; although a series of CER NS bilayers were studied with acyl chain lengths ranging from C_{12}−C_{20}, the simulations were limited in time scale, capturing only 20 ns, which may not be sufficient for a preassembled bilayer to fully relax itself from its initial state. Additionally, the authors did not provide the parameters used for the functional groups in the CER lipids that are absent from the CHARMM lipid topology. In more recent work, Noro and co-workers,[26,27,33] using the united atom model adapted from the GROMOS force field of Berger,[23] studied the interaction of dimethylsulfoxide (DMSO) with gel-phase bilayers of CER NS C_{24} and calculated the free energy of pore formation in both CER NS and CER NS/DMSO systems. Again, however, we note that the time scale considered was rather limited, with run times of only 20 ns after initial relaxation. Subsequently, the same authors studied a preassembled bilayer composed of CER NS, cholesterol, and a saturated free fatty acid 24 carbons in length, finding that cholesterol caused bilayer compression and interdigitation of the CER tails in the two opposing bilayer leaflets.[28−30]

From the extensive simulation studies of phospholipid bilayers, it has been well established that the GROMOS[34,35] and CHARMM[36,37] force fields are robust, and thus, a certain level of transferability to CERs is expected. However, small, but non-negligible, differences between the two force fields and with experiment are found for phospholipid systems with regards to properties such as the electron density profile and APL,[34,35,38] and considerable efforts have been made to further optimize these parameters to provide better agreement with experiment. For example, Chandrasekhar et al.[34] tested the GROMOS96 aliphatic alkane parameter set 45A3 with simulations of a dipalmitoyl phosphatidylcholine (DPPC) bilayer at 323 K. When comparing the average APL with experimental values, they found that GROMOS96 predicted an APL below the lowest reported experimental value; however, a later version of the GROMOS force field (G53A6 parameter set)[35] was found to greatly improve the fluidity of the bilayers, reducing this deviation. Similarly, Sonne et al.[37] modified the original CHARMM27 topology (named CHARMM27r) by proposing new partial charges for the atoms in the DPPC headgroup. Using the modified force field, a DPPC bilayer was studied and an APL of ∼60 Å^2 (compared to 48 Å^2 with CHARMM27) was obtained, which is ∼4−5 Å^2 smaller than the experimental value.[39] Motivated by the fact that CHARMM27r systematically yielded values of the APL that were smaller than experimental estimates and predicted the formation of gel-like bilayers well above the experimentally determined gel transition temperature, Klauda et al.[36] proposed a new lipid parameter set (which was subsequently included in the most recent update to the CHARMM force field, CHARMM36). Select torsional, Lennard-Jones, and partial charge parameters were modified by using, as reference, both quantum mechanical and experimental data; the changes were validated through the study of six phospholipids, including DPPC. The modifications were shown to provide improvements to properties such as the APL at zero tension, structure factor, NMR order parameters, and dipole electrostatic potential, as compared to the CHARMM27r parameter set. To evaluate the accuracy of the available simulation models, Piggot, et al.[38] simulated DPPC and 1-palmitoyl-2-oleoyl-sn-glycero-3-phosphocholine (POPC) bilayers using five freely available force fields that have been commonly used to model lipid bilayers, including force fields based upon GROMOS[23] and CHARMM36.[36] This work demonstrated that some bilayer properties have pronounced force field dependence, while

dx.doi.org/10.1021/ct400431e | J. Chem. Theory Comput. 2013, 9, 5116−5126

others are less sensitive. For example, the volume and APL, as well as bilayer height, were found to be accurately reproduced in comparison with experimental data by most of the force fields studied, while lipid diffusion showed striking differences depending on the force field used.

Despite the improvements in the GROMOS and CHARMM force fields for phospholipid bilayer simulations, it is unclear which force field is most appropriate for CERs, as neither has been specifically optimized for these systems and a direct side-by-side comparison of the force fields, both with each other and with experiments, is not yet available. Furthermore, while the literature does contain results of CER simulations using a CHARMM-based force field, the full parameter set used was not defined, making it impossible to use and evaluate this force field. In an effort to better understand the structural role of CERs in lipid bilayers and to understand the role of headgroup chemistry, we propose additional force field parameters for CHARMM to enable the simulation of CER NS and NP bilayers and compare the simulation results to those obtained from simulations with the Berger[23] modified version of the GROMOS force field. CER NS was chosen for this study because it is the most abundant ceramide species in human stratum corneum, it has been previously examined in simulation, and it has also been studied extensively in experiments[40−42] providing information regarding structural ordering and phase transitions. CER NP, the phytosphingosine counterpart of CER NS, is studied to assess, in a broad sense, the role of headgroup chemistry on bilayer properties. The remainder of the paper is organized as follows. In section II, the force fields, simulation methodology, and analysis methods are presented, including a detailed description of the headgroup partial charges and missing parameters for CHARMM-based simulation of CERs. In section III, results for bilayers composed of CER NS are reported, comparing the structural behavior and phase transitions predicted by both the CHARMM- and GROMOS-based force fields with experiment. Additionally, section III reports the properties of the bilayers formed by CER NP and compared to CER NS and experiment, with an emphasis on changes to hydrogen bonding resulting from headgroup structure. In section IV, we provide concluding remarks.

II. SIMULATION METHOD

2.1. Force Fields. Here, models based on the all-atom CHARMM force field[36,37,43−45] and the united-atom GROMOS force field[23,34,35] have been applied to simulate the CER lipid bilayers. Specifically, two systems have been studied: CER NS C_{16} and CER NP C_{16}, where both the fatty acid tail and the sphingosine/phytosphingosine tails are 16 carbons in length (note that the sphingosine/phytosphingosine tail is technically composed of 18 carbons, but the first 2 carbons are considered to be part of the headgroup region). Since both CHARMM and GROMOS are incomplete, in that they do not contain all the parameters required to study CERs, for clarity, we first provide details of the extended force fields used in this work.

All-Atom CHARMM-Based Force Field. Schematics of the all-atom CER NS are shown in Figures 1a and 2a, and CER NP in Figures 1b and 2c. The parameters for the lipid tails and OH groups are taken from the CHARMM36 topology files.[36] Although the CHARMM force field is extensive, it has not been parametrized specifically for lipids containing an amide group. In order to determine the missing parameters, *ab initio* calculations were performed to obtain the force constants and equilibrium distances/angles of atomistic CER NS and NP molecules. The electron structure was also obtained in order to determine the atomic partial charges. A detailed description of the procedure employed is included in the Supporting Information. The partial charges of the head groups are summarized graphically in Figure 1a and b, for CER NS and NP, respectively. The missing dihedral parameters and van der Waals parameters for the CER amide group were taken from the peptide bond parameters of protein force field;[44] bonded parameters were validated against the *ab initio* calculations, the details of which are also provided in the Supporting Information. The TIP3P[46] water model was used. Throughout the rest of this paper, we will refer to this extended version of the CHARMM force field simply as CHARMM-CER.

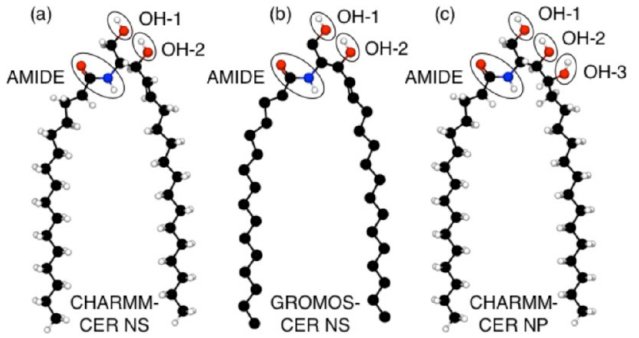

Figure 2. Schematic of the (a) CHARMM-CER NS model; (b) GROMOS-CER NS model; and (c) CHARMM-CER NP model. We note that even though GROMOS is a united-atom force field, the GROMOS-CER model includes explicit hydrogens on the amide, OH-1, and OH-2 groups. Gray atoms represent carbon atoms in a double bonded configuration.

United-Atom GROMOS-Based Force Field. Like CHARMM, GROMOS parameters have not been derived purposely for ceramide headgroup atoms. Specifically, there are no parameters explicitly stated for the amide group shown in Figure 2b. The force field used in this work comes from Berger,[23] who adapted the united atom GROMOS force field for the study of CERs; we briefly summarize this forcefield below. Note, in the GROMOS force field, the aliphatic tails are treated as united atoms (i.e., no explicit hydrogens) while the hydrogens bonded to oxygens and nitrogen in the headgroup are accounted for explicitly. Bonded and nonbonded interaction parameters used for atoms in the amide group were taken from the peptide nitrogen in the GROMOS87 parameter set and the hydrocarbon tails employ a Ryckaert−Bellemans potential,[47] which was used to better reproduce the experimental APL in DPPC bilayer simulations.[23] The partial charges for the headgroup atoms were taken from the side chain of serine, as in Mombelli et al.,[48] while the united atom carbons in the tail are charge-neutral. The atoms were broken into small, neutral charge groups to prevent discontinuities in the potential at the cutoff. The charge groups were taken to be as small as possible; for example, the nitrogen and hydrogen in the amide group make up a charge group, and each united atom carbon in the tail represents a single charge group. The simple point charge (SPC) water model[49] was used. For simplicity, henceforth this extended version of the GROMOS force field will be referred to as GROMOS-CER.

2.2. Simulation Details. *CHARMM-CER.* Atomistic models of hydrated CER bilayers were simulated using the LAMMPS[50,51] simulation engine. For all CHARMM-CER

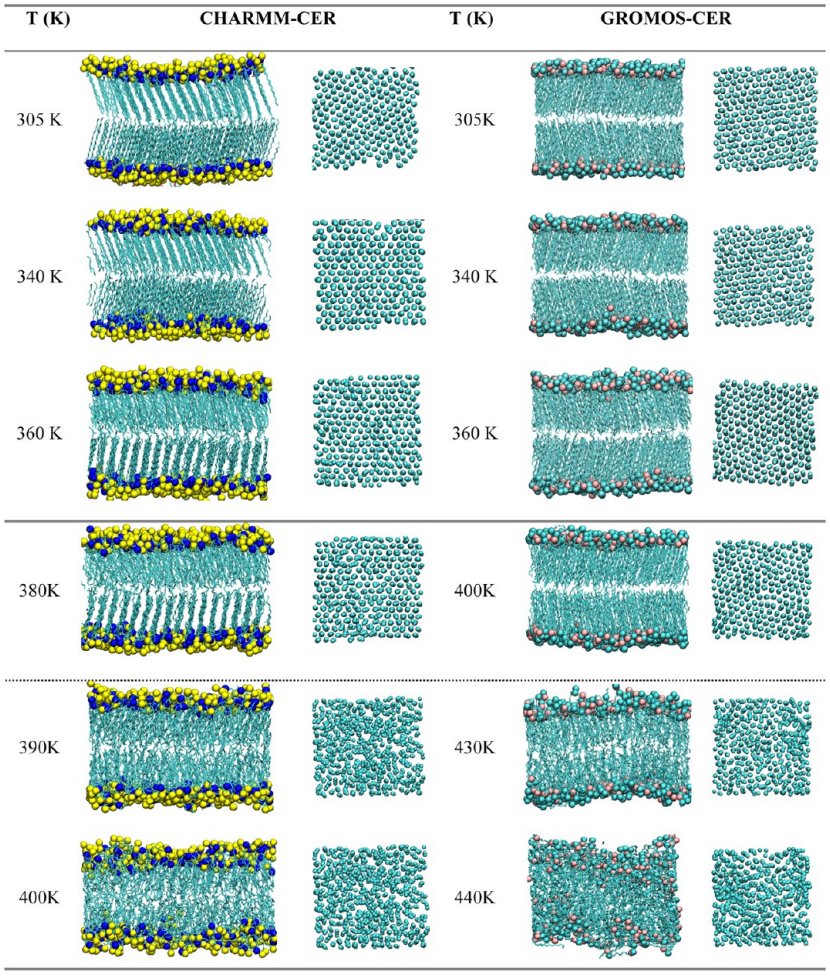

Figure 3. Snapshots of the observed phases for CER NS along the order−disorder transition. The horizontal dotted line demarkates gel phase bilayers (above) from liquid-like bilayer phases (below). Note water is removed for clarity and hydrogens removed from tail groups. In all cases, the figure at left is the side view of the bilayer and the figure at right is oriented to highlight the in-plane ordering of the tails segments.

systems, 100 molecules were placed in each leaflet of a preassmbled bilayer and then solvated with 10 000 water molecules. In order to relax each system, the temperature was increased from 0 to 305 K within the NVE ensemble using velocity rescaling; the time step was gradually increased to 1.0 fs in order to avoid energetic problems due to atomistic overlap. Simulations were run for 30 000 steps at which point the simulations were switched to the NPT anisotropic ensemble (Nosé−Hoover style non-Hamiltonian equations of motion from Shinoda et al.[52]) at a pressure of 1 atm, where pressure control is applied independently in each direction. The long-range electrostatic interactions were calculated through a particle−particle particle-mesh (PPPM) solver with a cutoff of 12 Å.[53] A time step of 1.0 fs was used during the NPT stage, where all simulations were run for at least 100 ns to ensure sufficient sampling within the steady state regime; specifically, CER NS was run for 107 ns and CER NP for 105 ns. Data for the APL, bilayer height, and system energy were collected during the last 30 ns to ensure a steady state had been reached.

To examine the thermotropic behavior (i.e., determine phase transitions as a function of temperature), an equilibrated bilayer structure at 305 K (run previously for >100 ns) was heated at a rate of 5 K/ns until bilayer rupture using the NPT ensemble with the same parameters described above. Cooling curves were started from a temperature just below the gel-to-liquid transition and cooled at a rate of 5 K/ns. As discussed in detail below, good agreement is found in the measured properties between the simulations run for >100 ns at a constant temperature of 305 K and the systems cooled to 305 K from just below the gel-to-liquid transition.

GROMOS-CER. The GROMOS-CER model was simulated using the GROMACS simulation engine.[54] The initial structure was constructed in the same manner as the CHARMM-CER bilayer, again using 100 lipids/leaflet. A steepest descent energy minimization run was performed to relax the initial configuration, followed by a 100 ps NVT equilibration at 305 K. The systems were then simulated for 100 ns in the NPT ensemble at 305 K and 1 atm using a Berendsen thermostat with anisotropic pressure coupling. A 2 fs time step was used. All interactions were cutoff at 12 Å and all bonds were constrained using the SHAKE algorithm. The simulation procedure employed replicates the reported procedures used in prior united atom CER studies by Notman et al.[27] Again, data were collected during the final 30 ns of simulation to ensure a steady state had been reached. Similar to simulations with the CHARMM-CER force field, thermotropic behavior was examined by heating an equilibrated bilayer structure at a rate of 5 K/ns from 305 K until bilayer rupture in the NPT ensemble. Cooling simulations were started from a temperature just below the gel-to-liquid transition and cooled at a rate of 5

dx.doi.org/10.1021/ct400431e | J. Chem. Theory Comput. 2013, 9, 5116−5126

K/ns; again, good agreement is found between systems that were run at a constant temperature of 305 K for 100 ns and those that were cooled from higher temperature.

It is important to note that both the SPC and TIP3P water models employed here have previously been shown to agree well with experiment with regards to density and heat of vaporization, even at the boiling point and our simulations show no evidence of anomalous behavior associated with the water models at elevated temperatures.[55]

2.3. Analysis. To provide a robust understanding of the lipid bilayers, several different metrics were used to quantify the structural ordering, determine phase transitions, and compare directly with experiment. The APL, a commonly reported quantity describing the compactness of the bilayer, was calculated by dividing the interfacial area of the bilayer (i.e., the *xy* plane) by the number of lipids in each leaflet. The bilayer thickness, also commonly reported in experimental and simulation studies, was calculated as the difference in *z*-values (bilayer normal direction) where the water density drops from its bulk value to $1/e$ of its bulk value.[27] The nematic order parameter, S_2,[56] of the tails was calculated to quantify the global orientational order of the tails, allowing a clear determination of gel vs fluid bilayers. A value of S_2 approaching unity indicates that the tails are in an ordered crystalline nematic structure suggesting a gel-like bilayer, and in this case, a value of $S_2 < 0.8$ (determined via visual inspection for the systems at hand) tends to indicate a more liquid-like ordering of the tails suggesting a fluid-like bilayer. The 2-d global hexagonal order parameter[57,58] (i.e., global in that it quantifies long-range hexagonal order) was also calculated to quantify the in-plane ordering of the tails. The hexagonal order parameter lies in the interval [0,1], where the upper bound corresponds to perfect hexagonal arrangement, and the magnitude of the value relates proportionally to the quality of the ordering. The tilt angle of the lipid tails relative to the bilayer normal was also quantified, where a tilt angle of 0° indicates that the tails are parallel to the bilayer normal. Additionally, the heat capacity, C_p, was calculated from the simulations performed as a function of temperature by taking the derivative of enthalpy with respect to temperature. A detailed description of the calculation of each of these metrics is provided in the Supporting Information.

III. RESULTS AND DISCUSSION

Comparison of CHARMM-CER and GROMOS-CER Force Fields for C_{16} CER NS at 305 K. As a first comparison of the CHARMM-CER and GROMOS-CER force fields, the bilayer structural properties are examined at a constant temperature of 305 K, as this is the physiologically relevant temperature of skin. Simulation snapshots of CER NS after 100 ns of simulation time are plotted for the CHARMM-CER force field and the GROMOS-CER force field in Figure 3. Visually, similar results are observed, where both force fields demonstrate stable, well ordered bilayer structures, with clear orientational ordering along the molecular axis of the tails and hexagonal ordering between neighboring tails in the planar direction.

To provide a quantitative comparison of the behavior, the APL, bilayer thickness, and chain tilt angle relative to the bilayer normal are calculated and summarized in Table 1. CHARMM-CER results in bilayers with a larger APL, smaller thickness, and a larger tilt angle than the GROMOS-CER force field. The difference in the bilayer thickness predicted from each force field can be attributed to the difference in the tilt angles, as a system with a larger tilt angle and identical tail length will demonstrate a smaller bilayer thickness.

Table 1. APL, Bilayer Height and Tilt Angle of CER Bilayers from the Constant Temperature Simulations

	APL (Å^2)	bilayer thickness (Å)	tilt angle (deg)
CHARMM-CER	42.4 ± 0.2	42.5 ± 0.5	24.3 ± 0.9
GROMOS-CER	39.8 ± 0.2	43.7 ± 0.4	17 ± 1

Based on X-ray diffraction experiments of pure, hydrated CER NS, Shah et al.[40] report a lamellar structure with a bilayer repeat distance of 46.9 Å at 299 K. In this regard, it would appear that both force fields underestimate the bilayer height slightly; however, it is important to note that the bilayer thickness can be calculated in multiple ways (see Supporting Information), and thus, the small differences seen here may instead be related to the methodological choice rather than a deficiency in the models. Using surface pressure-potential-molecular area isotherms, Scheffer et al.[59] calculated the APL of a CER NS monolayer to be 40 Å^2, Brockman et al.[60] calculated 37.8 Å^2, and Löfgren and Pascher[13] calculated 42 Å^2, which are all consistent with the values obtained from the two force fields. We also note that, in the simulations performed by Metcalf and Pandit[31] at 323 K, an APL of ∼44 Å^2 for pure CER and a tilt angle ∼26 degrees for a mixture of 90% CER NS and 10% SM were reported, which are consistent with our results from the CHARMM-CER force field.

Phase Transitions for CER NS C_{16}. As further comparison/validation of the two force fields, temperature scans are employed to examine the phase transitions as they compare to experiment.[8,40−42,61,62] Additionally, it is important to note that when modeling the stratum corneum, mixtures of different CERs, cholesterol, and free fatty acids with a range of tail lengths are present, which is likely to result in some level of spatial hetereogeneity, where, for example, gel and fluid-like tail segments exist simultaneously in different regions of the bilayer.[7,16,19,63,64] To be confident a given force field will provide dependable results for mixtures, it is important to investigate the thermotropic behavior, as temperature scans will enable sampling of different structural conformations of the tails. For both force fields, equilibrated bilayer structures were heated from 305 K until bilayer rupture; similarly, systems were cooled from below the main phase transition to 305 K.

Figure 3 presents simulation snapshots of CER NS bilayers as a function of temperature for heating runs conducted with both force fields. Visually, a clear transition from an ordered gel bilayer to a fluid-like bilayer occurs at ∼390 K and ∼430 K for simulations performed with the CHARMM-CER and GROMOS-CER force fields, respectively. This transition from gel- to liquid-like behavior is consistent with the trends reported in the prior simulation studies of Notman et al.,[27] where an ordered hexagonal arrangement of the lipid tails was observed at lower temperature state points of 283 and 323 K and liquid-like ordering at a higher temperature of 363 K, although we note that this prior work considered CER NS with a longer fatty acid tail (24 carbons) than studied here.

To provide a clearer picture of the behavior, the nematic order parameter, hexagonal order parameter, APL, tilt angle, bilayer height, and the heat capacity, C_p, are calculated and plotted in Figure 4 as a function of temperature. Focusing first on the C_p, two distinct peaks are found at 358 K and 383 K in the heating curve for CHARMM-CER system, and a peak is seen at ∼348 K in the cooling curve. Evidence of only a single

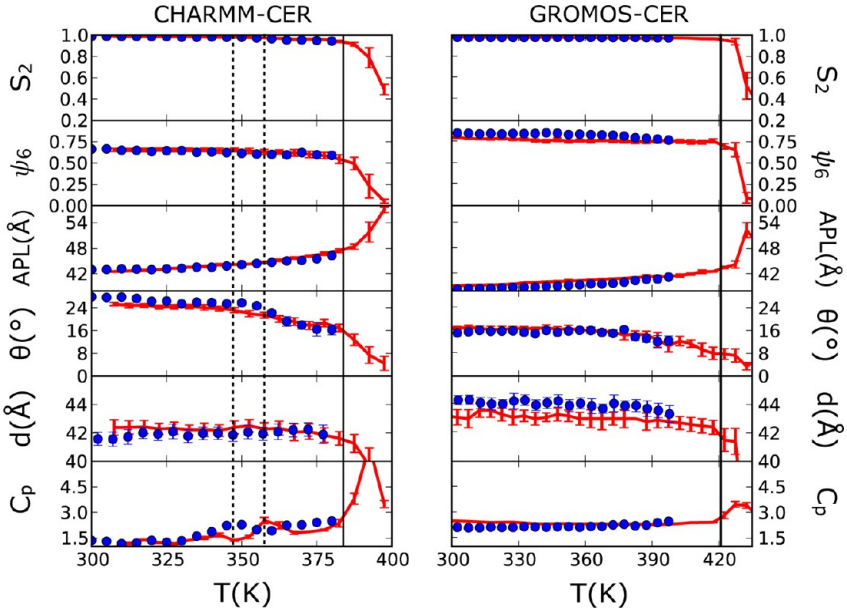

Figure 4. Structural and thermodynamic properties for CER NS bilayer along the order−disorder transition. (a) S_2 order parameter. (b) Hexagonal order parameter. (c) APL. (d) Tilt angle. (e) Bilayer height. (f) Heat capacity. The left column presents results from the CHARMM-CER force field and right column presents results from the GROMOS-CER force field. The solid lines represent the estimated gel-to-liquid phase transition temperature and dotted lines highlight the secondary peak in the heat capacity. The red lines correspond to the heating curve and the blue to the cooling curve.

transition (i.e., a single peak in C_p) at 428 K is found for the GROMOS-CER force field. These peaks appear to correlate well with changes in the various structural metrics, discussed below, and the estimated transitions are highlighted as vertical lines in Figure 4. Additionally, we note that, at 305 K, both heating and cooling data closely agree, providing additional validation of the robustness of the simulations presented prior (i.e., the initial structure did not strongly influence bilayer properties for the 100 ns runs).

For the CHARMM-CER force field, both the S_2 and hexagonal order parameters for the lipid tails show a clear drop at temperatures higher than ∼380 K. This corresponds to the loss of orientational and in-plane ordering of the tails and the formation of a bilayer with a fluid-like tail structure, consistent with visual inspection (see Figure 3); this transition is closely coupled to the large peak in the heat capacity that occurs above ∼380 K. Similar behavior is seen in the GROMOS-CER simulations, however, at an elevated temperature of ∼420 K.

The tilt angle for the CHARMM-CER system appears to demonstrate a hysteresis bounded by the two smaller peaks in heat capacity (348 and 358 K, shown as dashed lines in Figure 4). Typically, a hysteresis of ±15 K is reported when passing through the transitions of measurable quantities in simulation,[65] consistent with these results; other bilayer systems, such as phospholipids and bolaamphiphiles, have also been reported to have significant temperature hysteresis when comparing the heating and cooling scan.[66−68] As discussed in the literature,[66−68] the main reason for the hysteresis is that the reformation of the more ordered structure is kinetically limited. Performing the same examination of the GROMOS-CER simulations (Figure 4, right column), only a single transition appears evident at ∼420 K when considering the order parameters, heat capacity, and visual inspection. Only the tilt angle appears to show any temperature dependence prior to the gel-to-fluid bilayer transition, although at temperatures where both experiment and CHARMM-CER do not predict gel-like bilayers.

Comparing with experiment, the CHARMM-CER results appear to agree quite well with the calorimetric work of Chen et al.,[61] who performed Fourier transform infrared (FTIR) spectroscopy and differential scanning calorimetry (DSC) studies of CER NS. The main order−disorder transition temperature was reported to be 366.1 ± 1 K, in closer agreement with CHARMM-CER (∼380 K) than GROMOS-CER (∼420 K). We note that it is expected that the simulated heating scans will predict slightly elevated transition temperatures (e.g., by as much as 15 K compared to cooling[65]), especially given the rather "fast" heating rates used in simulations compared to experimental studies; taking this into account brings the CHARMM-CER force field in very close agreement with experiment. CHARMM-CER also provides good agreement with the work of Shah and Atienza,[42] who reported two transitions within the ordered regime at ∼350 K and ∼355 K for experiments of nonhydroxy fatty acid CERs; these transitions are in close agreement with the peaks observed at ∼348 and ∼358 K in C_p and the hysteresis in tilt angle in the CHARMM-CER simulations. Similarly, by examining the methylene stretching and scissoring modes, Chen et al.[61] observed a solid−solid phase transition at similar temperatures (∼340−345 K) resulting from chain packing alterations. However, in their work, the nature of the transition was associated with a change from orthorhombic (higher temperature) to hexagonal (lower temperature) subcells; in our simulations, no evidence of a hexagonal to orthorhombic transition is observed, although, we note that CHARMM-CER does predict alterations to the tail tilt-angle.

While there is consensus in the literature that the CER lipid tails are well ordered, the packing pattern is not completely agreed upon.[8,41,61,62,64] For example, at physiologically relevant temperatures, there is evidence of hexagonal[41] and orthorhombic packing,[62] as well as mixtures thereof.[69] While these

dx.doi.org/10.1021/ct400431e | J. Chem. Theory Comput. 2013, 9, 5116−5126

results seem to disagree, it is important to consider that the orthorhombic phase is hexagonal in nature (i.e., hexagonal, but "compressed" in one direction) and, for CER NS, it is suggested that the characteristic length scales in the orthorhombic phase differ by only ~10%.[7] As such, the differences between these phases may ultimately be very sensitive to slight differences between experimental procedures and/or simulation models/procedures.

Properties of CER NP C_{16}. As CHARMM-CER appears to more accurately model the behavior of CER NS, it was chosen for examination of the behavior of CER NP. To first provide a validation of CHARMM-CER for CER NP, a temperature scan was performed to determine the order−disorder transition for comparison with experiment. Similar to the CER NS temperature scan, the thermotropic behavior was investigated by heating from an equilibrated bilayer structure at 305 K (run for 105 ns), until bilayer rupture. The nematic order parameter, hexagonal order parameter, APL, tilt angle, bilayer height, and the heat capacity, C_p, are calculated and plotted in Figure 5.

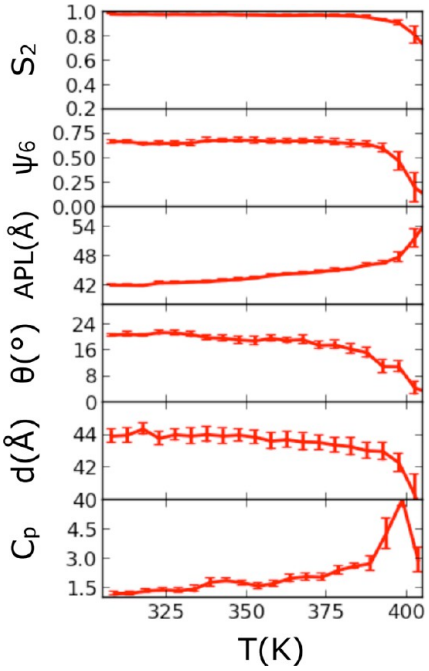

Figure 5. Structural and thermodynamic properties for CER NP bilayer with CHARMM-CER force field along order−disorder transition.

From these measurements, it appears that CER NP transitions from a gel to liquid bilayer state is at ~390−395 K, which is roughly 10−15 K higher than CER NS. This shift in the transition temperature is consistent with experiment; specifically, Garidel et al.[9] reported a main solid−liquid phase transition at 383 K and Rerek, et al.[8] reported chain melting at 388 K; recall, the main transition temperature of CER NS was reported to be 366 K.[61]

Comparisons of the Structural Differences between Head Groups: CER NS versus NP. Table 2 reports various structural properties of CER NS and NP at 305 K. We find that CER NP predicts a less tilted but thicker bilayer than CER NS, although both phases have similar APLs and values of the order parameters. These differences in tilt angle are surprising, given that CER NP and NS differ only in the replacement of an alkene functional group by a third hydroxy group (see Figures 1 and 2). Although fewer experimental measurements of the structural properties exist for CER NP compared to CER NS, surface pressure-potential-molecular area isotherms of CER NP monolayers conducted by Löfgren and Pascher[13] calculated the APL to be 48 Å^2 at zero surface tension, suggesting CHARMM-CER underpredicts this spacing (note, in these experiments, the APL drops rapidly to 42 Å^2 when the applied surface tension is increased to 30 dyn/cm). However, given that the APL for both simulated systems is roughly the same but CER NP has a larger bilayer thickness, this indicates that CER NP tail segments have a larger volume per lipid (i.e., larger accessible space per tail) than CER NS, consistent with the conclusion from IR spectroscopy studies that phytosphingosines pack less tightly than sphingosines.[8]

To further investigate the differences between CER NS and NP, the hydrogen bonds formed by the AMIDE and OH groups between lipids (see labels given in Figure 2), as well as between the lipids and water, have been determined and are reported in Table 3. As might be anticipated, due to the additional OH group, CER NP is found to have more hydrogen bonds than CER NS. This is consistent with the work of Rerek et al.,[8] who found that phytosphingosines have more significant hydrogen bonding than their sphingosine counterparts. In the 200-lipid bilayer system studied here, CER NP has, in total, 15% more hydrogen bonds than the CER NS bilayer of the same size and under the same thermodynamic conditions. With respect to the total number of hydrogen bonds formed by OH groups, there are 25% more hydrogen bonds in the CER NP bilayer than in the CER NS bilayer. This indicates that the additional OH group in CER NP plays a significant role in the formation of hydrogen bonds with surrounding hydrogen donors/acceptors, whereas the alkene group in CER NS is more stable in a hydrophobic environment.

Table 3. Number of Hydrogen Bonds among the Functional Groups in the Head Region and Water for CER NS and NP Bilayers from Simulation Run at 305 K, as Calculated from VMD[70] Using a Cutoff Distance of 3 Å and an Angle Criteria of 60°

	CER NS C_{16}		CER NP C_{16}	
group	lipid−lipid	lipid−water	lipid−lipid	lipid−water
AMIDE	14 ± 2.4	103 ± 9.1	15 ± 3.3	87 ± 7.1
OH	89 ± 7.2	422 ± 22.7	244 ± 11.7	361 ± 18.6
total	103 ± 9.6	525 ± 31.8	259 ± 15.0	448 ± 25.7

Table 2. APL, Bilayer Thickness, Tilt Angle, Nematic Order Parameter, and Hexagonal Order Parameter of CER NS and NP Bilayers from Simulations Run at 305 K

	APL (Å^2)	bilayer thickness (Å)	tilt angle (deg)	S_2	Hex OP
CER NS C_{16}	42.4 ± 0.2	42.5 ± 0.5	24.3 ± 0.9	0.980	0.68 ± 0.02
CER NP C_{16}	42.1 ± 0.2	44.1 ± 0.5	20.5 ± 0.8	0.980	0.68 ± 0.02

dx.doi.org/10.1021/ct400431e | J. Chem. Theory Comput. 2013, 9, 5116−5126

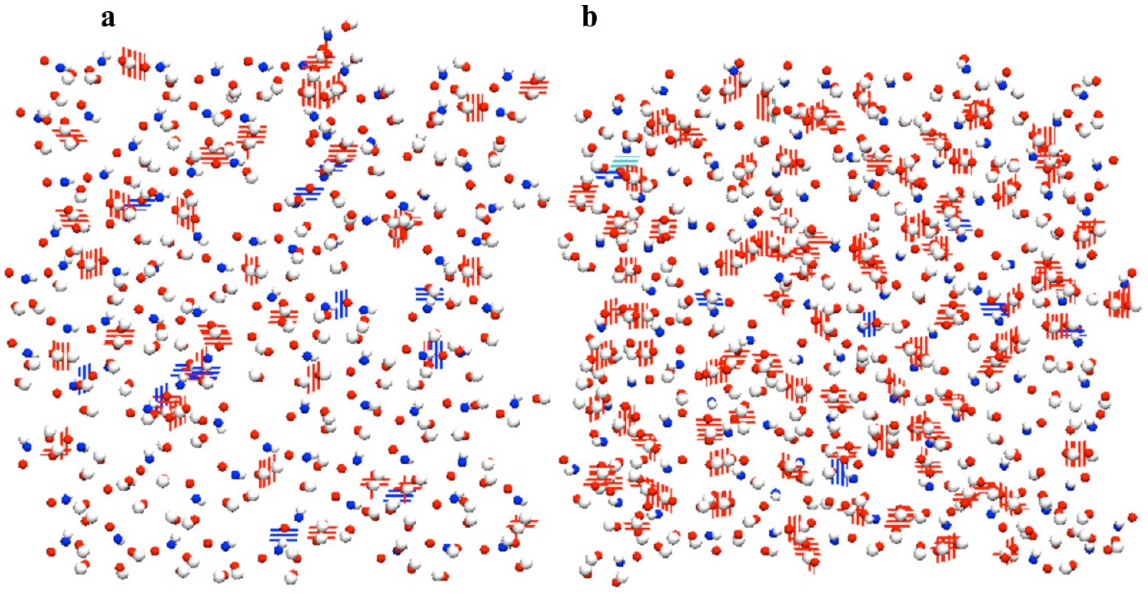

Figure 6. Lipid−lipid hydrogen bonding formed by AMIDE and OH groups. (a) CER NS leaflet; (b) CER NP leaflet. Blue, nitrogen; red, oxygen; white, hydrogen.

Notably, the distribution between lipid−lipid hydrogen bonds and lipid−water hydrogen bonds presents opposite trends for the two CERs studied. In CER NS, the most hydrogen bonds are formed with water (80%), with only 20% of the hydrogen bonds formed between lipids; while in CER NS this ratio becomes 40% versus 60%. The lipid−lipid hydrogen bonding snapshots for CER NS and NP are shown in Figure 6, from which we can see that the CER NP head groups form a tight and cohesive hydrogen bonding network, while CER NS shows more sparse and discontinuous intermolecular hydrogen bonds.

Experimentally, Garidel et al.[63] studied the microstructures of CER NS and CER NP via FTIR spectra and found that CER NS is characterized by weaker hydrogen bonding interactions between the head groups than CER NP, which is consistent with our observations. When comparing CERs of the same chain length, or chain length distribution, experimentally, one typically observes that the gel−liquid phase transition is higher for phytosphingosines than sphingosines.[9,41,61,62,71] Garidel et al.[63] hypothesized that this may result from the stronger interactions between the polar head groups. The simulations performed in this study support this hypothesis, where CER NP (phytosphingosine) is able to form a stronger hydrogen bond network compared to CER NS (sphingosine) and exhibits a slightly augmented order−disorder transition temperature.

Another notable point from Table 3 is that the simulations demonstrate that the AMIDE group in CER NS forms more hydrogen bonds than in CER NP, with ∼20% more AMIDE groups participating in the formation of the hydrogen bonding network. This may be due to the strong headgroup hydrogen bonding network that forms among the three OH groups in CER NP, making it less advantageous for the AMIDE to participate in the formation of hydrogen bonds.

In Figure 7, the distributions of the angle between the hydroxyl oxygen and connecting carbon bonds (C−O) and the bilayer normal in both the CER NS and CER NP systems are plotted for the OH-1 and OH-2 groups (see labels given in Figure 2). From Figure 7a, it is observed that the C−O angle

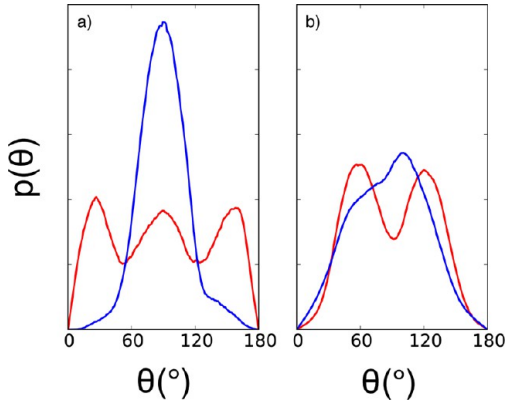

Figure 7. Distribution of angle between hydroxyl oxygen and connecting carbon relative to bilayer normal for CER NS and CER NP head groups. (a) C−O bond with OH-1; (b) C−O bond with OH-2. Red lines represent CER NS, and blue lines represent CER NP at T = 305 K.

for CER NS is evenly distributed at 25°, 90°, and 155°, suggesting two-thirds of the C−O bonds with OH-1 align perpendicularly while only one-third are in the horizontal direction. In comparison, the curves for CER NP are significantly more peaked with a higher intensity value at ∼90°. Thus, in CER NP systems, the C−O bond with OH-1 tends to be more horizontal relative to the bilayer normal. The C−O bond with the OH-2 group in both systems shows similar trends: C−O in CER NS distributes evenly at 60° and 120°, while for CER NP a single peak is seen at 95°. These results suggest that in CER NP, the C−O bonds adjacent to the OH groups adopt a more horizontal orientation, resulting in a flatter headgroup region at the lipid−water interface. This change in position appears to be the cause for the augmented hydrogen bonding network seen for CER NP.

The radial distribution function (RDF) has also been calculated to further compare the structural characteristics and headgroup arrangement in CER NS and NP bilayers. The RDFs of the nitrogen in the AMIDE group and oxygen in the

dx.doi.org/10.1021/ct400431e | J. Chem. Theory Comput. 2013, 9, 5116−5126

OH-1 and OH-2 group for CER NS and NP are shown in Figure 8.

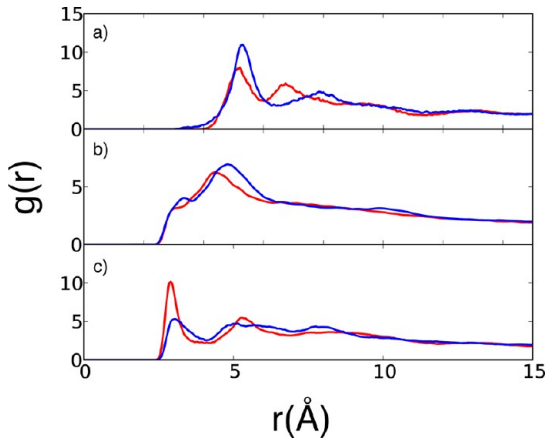

Figure 8. Head group RDFs for CER NS C_{16} and CER NP C_{16}. (a) Nitrogen−nitrogen RDF. (b) Oxygen−oxygen RDF for OH-1. (c) Oxygen−oxygen RDF for OH-2. Red lines represent CER NS and blue lines represent CER NP.

Figure 8a shows that CER NP has a higher intensity of the first peak in the nitrogen−nitrogen RDF than CER NS, while the peak position for the two lipids is very similar. This suggests that, for CER NP, the nitrogen atoms have, on average, more nearest neighbors than the nitrogen atoms in the CER NS system. Since the APL for both CER NP and CER NS bilayers is ∼42 Å^2, we can infer that the CER NP AMIDE groups tend to assemble together and form a more open polar interface than the CER NS system. This can also be seen by examining the position of the secondary peaks; CER NS has a minor peak at 6.25 Å while CER NP peaks around 7.4 Å. This measurement is consistent with the observation by Rerek et al.,[8] who proposed that the more open polar interface allows phytosphingosine CERs to form a stronger hydrogen bond network compared to sphingosine CERs.

While the RDF measurements in Figure 8b for OH-1 are similar for both systems, the measurements for OH-2 shown in Figure 8c differ significantly for CERs NS and NP. Although the spacing of the first two peaks is similar, the magnitude of the first peak in CER NS is approximately double that of CER NP. This suggests that, without the influence of the OH-3 group in the phytosphigosine tail, the OH-2 group in CER NS possesses more order than its counterpart in CER NP; the latter tends to form a loosely arranged structure. This is supported by the distribution of C−O angles reported in Figure 7, where OH-2 in CER NP adopts a more parallel arrangement, influencing this packing.

IV. CONCLUSIONS

The structure and thermotropic properties of CER NS bilayers have been compared using force fields based upon the CHARMM force field (CHARMM-CER), developed as part of this work, and the GROMOS force field (GROMOS-CER) modified by Berger.[23] We find that, at physiological conditions, both force fields demonstrate similar behavior for CER NS, consistent with the available experimental measurements; however, subtle differences between the force fields are seen with respect to bilayer height and tilt angle, where GROMOS-CER tends to predict more compact, less tilted structures than CHARMM-CER. Examination of thermotropic properties and comparison with experimental observations shows more significant differences between the two force fields. GROMOS-CER predicts a main gel−liquid phase transition at ∼420 K whereas CHARMM-CER predicts a transition at ∼380 K, more consistent with experiment. CHARMM-CER also resolves a subtle order−order phase transition at ∼350 K, consistent with experimental measurements, while this transition is absent in the GROMOS-CER simulations. Given that the stratum corneum is composed of more than a dozen different lipids, it is important that a force field that is capable of resolving the subtle structural differences and phase transitions in order to accurately model this layer. However, it is important to note that the increased accuracy of the proposed CHARMM-based force field comes with additional computational cost, which may place practical limits on the system size and time scale that can be efficiently examined. As such, the GROMOS-based force field will no doubt still play a vital role regarding the investigation of CERs, particularly given that it could be optimized to better capture thermotropic behavior.

When examining the role of headgroup chemistry by comparing CER NS to NP, our results find that the substitution of OH-3 in place of the alkene bond changes not only the neighboring OH-2 from a perpendicular to a horizontal orientation but also induces the formation of a more significant hydrogen bonding network, resulting in much stronger intermolecular headgroup interactions compared with that seen in CER NS. These structural differences lead to a higher gel−liquid phase transition temperature for the phytosphingosines (CER NP) compared to sphingosines (CER NS), consistent with experiment. Slight changes in the CER headgroup chemistry appear to have a dramatic influence on the morphological features and thermodynamic properties of the lipid bilayers, underscoring the importance of performing computational investigations of the molecular-level behavior of the different classes of CERs found in the stratum corneum.

■ ASSOCIATED CONTENT

Ⓢ Supporting Information

A detailed description of the procedure employed to develop the CHARMM-CER force field with *ab initio* calculations is provided. The parameters used for the amide group in CERs, including the force constants and equilibrium distances/angles as well as the atomic partial charges are given. A description of the calculation of each of the bilayer metrics is also provided. This material is available free of charge via the Internet at http://pubs.acs.org.

■ AUTHOR INFORMATION

Corresponding Author

*E-mail: c.mccabe@vanderbilt.edu.

Notes

The authors declare no competing financial interest.

■ ACKNOWLEDGMENTS

This work was supported by Grant No. R01 AR057886-01 from the National Institute of Arthritis and Muscoskeletal and Skin Diseases. Computational resources were provided by the National Energy Research Scientific Computing Center, supported by the Office of Science of the Department of Energy under Contract No. DE-AC02-05CH11231. We also

acknowledge Annette Bunge and Joke Bouwstra for useful discussions.

REFERENCES

(1) Schaefer, H.; Redelmeier, T. E. *Skin Barrier: Principles of Percutaneous Absorption*; Karger: New York, 1996; 31−49.

(2) Downing, D. T.; Stewart, M. E.; Wertz, P. W.; Colton Vi, S. W.; Strauss, J. S. Skin Lipids. *Comp. Biochem. Physiol., Part B: Biochem. Mol. Biol.* **1983**, *76*, 673−678.

(3) Robson, K. J.; Stewart, M. E.; Michelsen, S.; Lazo, N. D.; Downing, D. T. 6-Hydroxy-4-Sphingenine in Human Epidermal Ceramides. *J. Lipid Res.* **1994**, *35*, 2060−2068.

(4) Bleck, O.; Abeck, D.; Ring, J.; Hoppe, U.; Vietzke, J.-P.; Wolber, R.; Brandt, O.; Schreiner, V. Two Ceramide Subfractions Detectable in Cer(AS) Position by HPTLC in Skin Surface Lipids of Non-lesional Skin of Atopic Eczema. *J. Invest. Dermatol.* **1999**, *113*, 894−900.

(5) Stewart, M. E.; Downing, D. T. A New 6-Hydroxy-4-Sphingenine-Containing Ceramide in Human Skin. *J. Lipid Res.* **1999**, *40*, 1434−1439.

(6) Wertz, P. W. Lipids and Barrier Function of the Skin. *Acta Derm.-Venereol.* **2000**, 7−11.

(7) Pilgram, G. S. K.; Vissers, D. C. J.; van der Meulen, H.; Pavel, S.; Lavrijsen, S. P. M.; Bouwstra, J. A.; Koerten, H. K. Aberrant Lipid Organization in Stratum Corneum of Patients with Atopic Dermatitis and Lamellar Ichthyosis. *J. Invest. Dermatol.* **2001**, *117*, 710−717.

(8) Rerek, M. E.; Chen; Markovic, B.; Van Wyck, D.; Garidel, P.; Mendelsohn, R.; Moore, D. J. Phytosphingosine and Sphingosine Ceramide Headgroup Hydrogen Bonding: Structural Insights through Thermotropic Hydrogen/Deuterium Exchange. *J. Phys. Chem. B.* **2001**, *105*, 9355−9362.

(9) Garidel, P. Calorimetric and Spectroscopic Investigations of Phytosphingosine Ceramide Membrane Organisation. *Phys. Chem. Chem. Phys.* **2002**, *4*, 1934−1942.

(10) Raudenkolb, S.; Hubner, W.; Rettig, W.; Wartewig, S.; Neubert, R. H. H. Polymorphism of Ceramide 3. Part 1: An Investigation Focused on the Head Group of N-Octadecanoylphytosphingosine. *Chem. Phys. Lipids* **2003**, *123*, 9−17.

(11) Raudenkolb, S.; Wartewig, S.; Neubert, R. H. H. Polymorphism of Ceramide 3. Part 2: A Vibrational Spectroscopic and X-ray Powder Diffraction Investigation of N-Octadecanoyl phytosphingosine and the Analogous Specifically Deuterated D(35) Derivative. *Chem. Phys. Lipids* **2003**, *124*, 89−101.

(12) Raudenkolb, S.; Wartewig, S.; Neubert, R. H. H. Polymorphism of Ceramide 6: A Vibrational Spectroscopic and X-ray Powder Diffraction Investigation of the Diastereomers of N-(α-hydroxyoctadecanoyl)-phytosphingosine. *Chem. Phys. Lipids* **2005**, *133*, 89−102.

(13) Löfgren, H.; Pascher, I. Molecular Arrangements of Sphingolipids. The Monolayer Behavior of Ceramides. *Chem. Phys. Lipids* **1977**, *20*, 273−284.

(14) Bouwstra, J. A.; Gooris, G. S. The Lipid Organization in Human Stratum Corneum and Model Systems. *Open Derm. J.* **2010**, *4*, 10−13.

(15) Bouwstra, J. A.; Gooris, G. S.; Dubbelaar, F. E. R.; Ponec, M. Phase Behavior of Stratum Corneum Lipid Mixtures Based on Human Ceramides: The Role of Natural and Synthetic Ceramide 1. *J. Invest. Dermatol.* **2002**, *118*, 606−617.

(16) Groen, D.; Gooris, G. S.; Bouwstra, J. A. Model Membranes Prepared with Ceramide EOS, Cholesterol and Free Fatty Acids Form a Unique Lamellar Phase. *Langmuir* **2010**, *26*, 4168−4175.

(17) Engelbrecht, T.; Hauss, T.; Suss, K.; Vogel, A.; Roark, M.; Feller, S. E.; Neubert, R. H. H.; Dobner, B. Characterisation of a New Ceramide EOS Species: Synthesis and Investigation of the Thermotropic Phase Behavior and Influence on the Bilayer Architecture of Stratum Corneum Lipid Model Membranes. *Soft Matter.* **2011**, *7*, 8998−9011.

(18) Engelbrecht, T. N.; Schroeter, A.; Hauss, T.; Deme, B.; Scheidt, H. A.; Huster, D.; Neubert, R. H. The Impact of Ceramides NP and AP on the Nanostructure of Stratum Corneum Lipid Bilayer. Part I: Neutron Diffraction and 2H NMR Studies on Multilamellar Models Based on Ceramides with Symmetric Alkyl Chain Length Distribution. *Soft Matter* **2012**, *8*, 6599−6607.

(19) Mao, G.; VanWyck, D.; Xiao, X.; Mack Correa, M. C.; Gunn, E.; Flach, C. R.; Mendelsohn, R.; Walters, R. M. Oleic Acid Disorders Stratum Corneum Lipids in Langmuir Monolayers. *Langmuir* **2013**, *29*, 4857−4865.

(20) Lyubartsev, A. P.; Rabinovich, A. L. Recent Development in Computer Simulations of Lipid Bilayers. *Soft Matter* **2011**, *7*, 25−39.

(21) Alwarawrah, M.; Dai, J.; Huang, J. Modification of Lipid Bilayer Structure by Diacylglycerol: A Comparative Study of Diacylglycerol and Cholesterol. *J. Chem. Theory Comput.* **2012**, *8*, 749−758.

(22) Srivastava, A.; Voth, G. A. Hybrid Approach for Highly Coarse-Grained Lipid Bilayer Models. *J. Chem. Theory Comput.* **2013**, *9*, 750−765.

(23) Berger, O.; Edholm, O.; Jahnig, F. Molecular Dynamics Simulations of a Fluid Bilayer of Dipalmitoylphosphatidylcholine at Full Hydration, Constant Pressure, and Constant Temperature. *Biophys. J.* **1997**, *72*, 2002−2013.

(24) Imai, Y.; Liu, X. L.; Yamagishi, J.; Mori, K.; Neya, S.; Hoshino, T. Computational Analysis of Water Residence on Ceramide and Sphingomyelin Bilayer Membranes. *J. Mol. Graphics Modell* **2010**, *29*, 461−469.

(25) Pandit, S. A.; Scott, H. L. Molecular Dynamics Simulation of a Ceramide Bilayer. *J. Chem. Phys.* **2006**, *124*, 7.

(26) Notman, R.; Anwar, J.; Briels, W. J.; Noro, M. G.; den Otter, W. K. Simulations of Skin Barrier Function: Free Energies of Hydrophobic and Hydrophilic Transmembrane Pores in Ceramide Bilayers. *Biophys. J.* **2008**, *95*, 4763−4771.

(27) Notman, R.; den Otter, W. K.; Noro, M. G.; Briels, W. J.; Anwar, J. The Permeability Enhancing Mechanism of DMSO in Ceramide Bilayers Simulated by Molecular Dynamics. *Biophys. J.* **2007**, *93*, 2056−2068.

(28) Das, C.; Noro, M. G.; Olmsted, P. D. Simulation Studies of Stratum Corneum Lipid Mixtures. *Biophys. J.* **2009**, *97*, 1941−1951.

(29) Das, C.; Olmsted, P. D.; Noro, M. G. Water Permeation through Stratum Corneum Lipid Bilayers from Atomistic Simulations. *Soft Matter.* **2009**, *5*, 4549−4555.

(30) Hoopes, M. I.; Noro, M. G.; Longo, M. L.; Faller, R. Bilayer Structure and Lipid Dynamics in a Model Stratum Corneum with Oleic Acid. *J. Phys. Chem. B.* **2011**, *115*, 3164−3171.

(31) Metcalf, R.; Pandit, S. A. Mixing Properties of Sphingomyelin Ceramide Bilayers: A Simulation Study. *J. Phys. Chem. B.* **2012**, *116*, 4500−4509.

(32) Chiu, S. W.; Vasudevan, S.; Jakobsson, E.; Mashl, R. J.; Scott, H. L. Structure of Sphingomyelin Bilayers: A Simulation Study. *Biophys. J.* **2003**, *85*, 3624−3635.

(33) den Otter, W. K.; Notman, R.; Anwar, J.; Noro, M. G.; Briels, W. J. Modulating the Skin Barrier Function by DMSO: Molecular Dynamics Simulations of Hydrophilic and Hydrophobic Transmembrane Pores. *Chem. Phys. Lipids* **2008**, *154* (Supplement), S2−S3.

(34) Chandrasekhar, I.; Kastenholz, M.; Lins, R. D.; Oostenbrink, C.; Schuler, L. D.; Tieleman, D. P.; van Gunsteren, W. F. A Consistent Potential Energy Parameter Set for Lipids: Dipalmitoylphosphatidylcholine as a Benchmark of the Gromos96 45a3 Force Field. *Eur. Biophys. J.* **2003**, *32*, 67−77.

(35) Poger, D.; Van Gunsteren, W. F.; Mark, A. E. A New Force Field for Simulating Phosphatidylcholine Bilayers. *J. Comput. Chem.* **2010**, *31*, 1117−1125.

(36) Klauda, J. B.; Venable, R. M.; Freites, J. A.; O'Connor, J. W.; Tobias, D. J.; Mondragon-Ramirez, C.; Vorobyov, I.; MacKerell, A. D.; Pastor, R. W. Update of the CHARMM All-Atom Additive Force Field for Lipids: Validation on Six Lipid Types. *J. Phys. Chem. B* **2010**, *114*, 7830−7843.

(37) Sonne, J.; Jensen, M.; Hansen, F. Y.; Hemmingsen, L.; Peters, G. H. Reparameterization of All-Atom Dipalmitoylphosphatidylcholine Lipid Parameters Enables Simulation of Fluid Bilayers at Zero Tension. *Biophys. J.* **2007**, *92*, 4157−4167.

(38) Piggot, T. J.; Pineiro, A.; Khalid, S. Molecular Dynamics Simulations of Phosphatidylcholine Membranes: A Comparative Force Field Study. *J. Chem. Theory Comput.* **2012**, *8*, 4593−4609.
(39) Nagle, J. F.; Tristram-Nagle, S. Structure of Lipid Bilayers. *Biochim. Biophys. Acta, Rev. Biomembr.* **2000**, *1469*, 159−195.
(40) Shah, J.; Atienza, J.; Dong, Z. X.; Shipley, G. G. X-ray Diffraction and Calorimetric Studies of Non-hydroxy Fatty-Acid (16−0) Ceramide. *Biophys. J.* **1994**, *66*, A288−A288.
(41) Shah, J.; Atienza, J. M.; Duclos, R. I.; Rawlings, A. V.; Dong, Z. X.; Shipley, G. G. Structural and Thermotropic Properties of Synthetic C16−0 (Palmitoyl) Ceramide—Effect of Hydration. *J. Lipid Res.* **1995**, *36*, 1936−1944.
(42) Shah, J.; Atienza, J. M.; Rawlings, A. V.; Shipley, G. G. Physical Properties of Ceramides Effect of Fatty Acid Hydroxylation. *J. Lipid Res.* **1995**, *36*, 1945−1955.
(43) Feller, S. E.; MacKerell, A. D. An Improved Empirical Potential Energy Function for Molecular Simulations of Phospholipids. *J. Phys. Chem. B.* **2000**, *104*, 7510−7515.
(44) MacKerell, A. D.; Bashford, D.; Bellott, M.; Dunbrack, R. L.; Evanseck, J. D.; Field, M. J.; Fischer, S.; Gao, J.; Guo, H.; Ha, S.; Joseph-McCarthy, D.; Kuchnir, L.; Kuczera, K.; Lau, F. T. K.; Mattos, C.; Michnick, S.; Ngo, T.; Nguyen, D. T.; Prodhom, B.; Reiher, W. E.; Roux, B.; Schlenkrich, M.; Smith, J. C.; Stote, R.; Straub, J.; Watanabe, M.; Wiorkiewicz-Kuczera, J.; Yin, D.; Karplus, M. All-Atom Empirical Potential for Molecular Modeling and Dynamics Studies of Proteins. *J. Phys. Chem. B.* **1998**, *102*, 3586−3616.
(45) Pastor, R. W.; MacKerell, A. D. Development of the CHARMM Force Field for Lipids. *J. Phys. Chem. Lett.* **2011**, *2*, 1526−1532.
(46) Jorgensen, W. L.; Chandrasekhar, J.; Madura, J. D.; Impey, R. W.; Klein, M. L. Comparison of Simple Potential Functions for Simulating Liquid Water. *J. Chem. Phys.* **1983**, *79*, 926−935.
(47) Ryckaert, J. P.; Bellemans, A. Molecular Dynamics of Liquid Alkanes. Farady Discussion. *Chem. Soc.* **1978**, *66*, 95−106.
(48) Mombelli, E.; Morris, R.; Taylor, W.; Fraternali, F. Hydrogen-Bonding Propensities of Sphingomyelin in Solution and in a Bilayer Assembly: A Molecular Dynamics Study. *Biophys. J.* **2003**, *84*, 1507−1517.
(49) Berendsen, H. J. C.; Postma, J. P. M.; van Gunsteren, W. F.; Hermans, W. F. Interaction Models for Water in Relation to Protein Hydration. In *Intermolecular Forces*; D. Reidel Publishing: Dordrecht, The Netherlands, 1981; pp 331−342.
(50) Lammps Molecular Dynamics Simulator, Http://Lammps.Sandia.Gov (accessed March 8, 2012).
(51) Plimpton, S. Fast Parallel Algorithms for Short-Range Molecular Dynamics. *J. Comput. Phys.* **1995**, *117*, 1−19.
(52) Shinoda, S. Mikami. Lammps NPT Barostat. *Phys. Rev. B.* **2004**, *69*, 134103.
(53) Hockney; R. W.; Eastwood, J. W. *Computer Simulation Using Particles*; Taylor & Francis: New York, 1989; 121−142.
(54) Kutzner, B.; van der Spoel, D.; Lindahl, E. Gromacs 4: Algorithms for Highly Efficient, Load−Balanced, and Scalable Molecular Simulation Hess. *J. Chem. Theory. Comput.* **2008**, *4*, 435−447.
(55) Jorgensen, W. L.; Jenson, C. Temperature Dependence of TIP3P, SPC, and TIP4P Water from NPT Monte Carlo Simulations: Seeking Temperatures of Maximum Density. *J. Comput. Chem.* **1998**, *19*, 1179−1186.
(56) Wilson, M. R. Determination of Order Parameters in Realistic Atom-Based Models of Liquid Crystal Systems. *J. Mol. Liq.* **1996**, *68*, 23−31.
(57) Keys, A. S.; Iacovella, C. R.; Glotzer, S. C. Characterizing Structure through Shape Matching and Applications to Self-Assembly. *Annual Review of Condensed Matter Physics, Vol 2* **2011**, *2*, 263−285.
(58) Keys, A. S.; Iacovella, C. R.; Glotzer, S. C. Characterizing Complex Particle Morphologies through Shape Matching: Descriptors, Applications, and Algorithms. *J. Comput. Phys.* **2011**, *230*, 6438−6463.
(59) Scheffer, L.; Solomonov, I.; Jan Weygand, M.; Kjaer, K.; Leiserowitz, L.; Addadi, L. Structure of Cholesterol/Ceramide Monolayer Mixtures: Implications to the Molecular Organization of Lipid Rafts. *Biophys. J.* **2005**, *88*, 3381−3391.
(60) Brockman, H. L.; Momsen, M. M.; Brown, R. E.; He, L. L.; Chun, J.; Byun, H. S.; Bittman, R. The 4,5-Double Bond of Ceramide Regulates Its Dipole Potential, Elastic Properties, and Packing Behavior. *Biophys. J.* **2004**, *87*, 1722−1731.
(61) Chen, H.-C.; Mendelsohn, R.; Rerek, M. E.; Moore, D. J. Fourier Transform Infrared Spectroscopy and Differential Scanning Calorimetry Studies of Fatty Acid Homogeneous Ceramide 2. *Biochim. Biophys. Acta: Biomembr.* **2000**, *1468*, 293−303.
(62) Moore, D. J.; Rerek, M. E.; Mendelsohn, R. FTIR Spectroscopy Studies of the Conformational Order and Phase Behavior of Ceramides. *J. Phys. Chem. B.* **1997**, *101*, 8933−8940.
(63) Garidel, P.; Foelting, B.; Schaller, I.; Kerth, A. The Microstructure of the Stratum Corneum Lipid Barrier: Midinfrared Spectroscopic Studies of Hydrated Ceramide/Palmitic Acid/Cholesterol Model Systems. *Biophys. Chem.* **2010**, *150*, 144−156.
(64) Moore, D. J.; Rerek, M. E.; Mendelsohn, R. Lipid Domains and Orthorhombic Phases in Model Stratum Corneum: Evidence from Fourier Transform Infrared Spectroscopy Studies. *Biochem. Biophys. Res. Commun.* **1997**, *231*, 797−801.
(65) Waheed, Q.; Tjornhammar, R.; Edholm, O. Phase Transitions in Coarse-Grained Lipid Bilayers Containing Cholesterol by Molecular Dynamics Simulations. *Biophys. J.* **2012**, *103*, 2125−2133.
(66) Holopainen, J. M.; Lemmich, J.; Richter, F.; Mouritsen, O. G.; Rapp, G.; Kinnunen, P. K. J. Dimyristoylphosphatidylcholine/C16:0-ceramide Binary Liposomes Studied by Differential Scanning Calorimetry and Wide- and Small-Angle X-ray Scattering. *Biophys. J.* **2000**, *78*, 2459−2469.
(67) Kohler, K.; Forster, G.; Hauser, A.; Dobner, B.; Heiser, U. F.; Ziethe, F.; Richter, W.; Steiniger, F.; Drechsler, M.; Stettin, H.; Blume, A. Temperature-Dependent Behavior of a Symmetric Long-Chain Bolaamphiphile with Phosphocholine Headgroups in Water: From Hydrogel to Nanoparticles. *J. Am. Chem. Soc.* **2004**, *126*, 16804−16813.
(68) Garidel, P.; Blume, A. Interaction of Alkaline Earth Cations with the Negatively Charged Phospholipid 1,2-Dimyristoyl-Sn-glycero-3-phosphoglycerol: A Differential Scanning and Isothermal Titration Calorimetric Study. *Langmuir* **1999**, *15*, 5526−5534.
(69) Ongpipattanakul, B.; Francoeur, M. L.; Potts, R. O. Polymorphism in Stratum Corneum Lipids. *Biochim. Biophys. Acta: Biomembr.* **1994**, *1190*, 115−122.
(70) Humphrey, W.; Dalke, A.; Schulten, K. VMD: Visual Molecular Dynamics. *J. Mol. Graph.* **1996**, *14*, 33−38.
(71) Garidel, P. Structural Organisation and Phase Behavior of a Stratum Corneum Lipid Analogue: Ceramide 3A. *Phys. Chem. Chem. Phys.* **2006**, *8*, 2265−2275.

SUPPLEMENTARY INFORMATION

Development of CHARMM-CER force field:

The *CHARMM-CER* forcefield was constructed based on the CHARMM all-atom force field.[1-3] While lipid parameters in CHARMM exist, they have not been derived specifically for ceramide (CER) lipids and no parameters are explicitly given for the amide group found in CERs, shown in Figure 2 of the main document. In order to determine the missing parameters, *ab initio* calculations were performed to obtain missing force constants and the equilibrium bond distances/angles in atomistic CER NS and NP molecules. The electron structure was also obtained to determine the atomic partial charges on the corresponding atoms. Dihedral parameters and van der Waals interactions were used directly from the peptide bond parameters in the CHARMM protein force field[1]. The sources for this extended version of the force field are summarized in Table S1.

Table S1. Force field development for CER lipids (*CHARMM-CER*)

Interactions	Hydrocarbon Tails	Hydroxyl Group	Amide Group
Bonds and Angles	CHARMM36 lipid topology	CHARMM36 lipid topology	*ab initio* calculation
Dihedrals	CHARMM36 lipid topology	CHARMM36 lipid topology	CHARMM36 protein force field, peptide group
van der Waals	CHARMM36 lipid topology	CHARMM36 lipid topology	CHARMM36 protein force field, peptide group
Partial charges	Quantum mechanics *ab initio* calculation		

Bonded interactions:

To calculate the missing bonded parameters, *i.e.,* bond stretching and angle bending, the molecular software package GAUSSIAN 09[4] was used to perform *ab initio* calculations with the B3LYP level of theory and the 6-31++G** basis set.

Eight random configurations of each molecule were generated with the molecular editor software package Avogadro[5, 6]. Since internal CH_2 groups along the tails are expected to contain a total neutral charge and the longest-range bonded interaction is a 1-4 dihedral, the CER molecules were truncated to tails of four carbons in length. The structure of the truncated CER NS is shown in Figure S1. A geometric optimization was then performed on each of the eight input data files to determine the equilibrium configuration, from which the force constants and equilibrium distances/angles were averaged; these values are reported in Table S2. Again, dihedral parameters were taken from the peptide bond in the CHARMM protein force field[1].

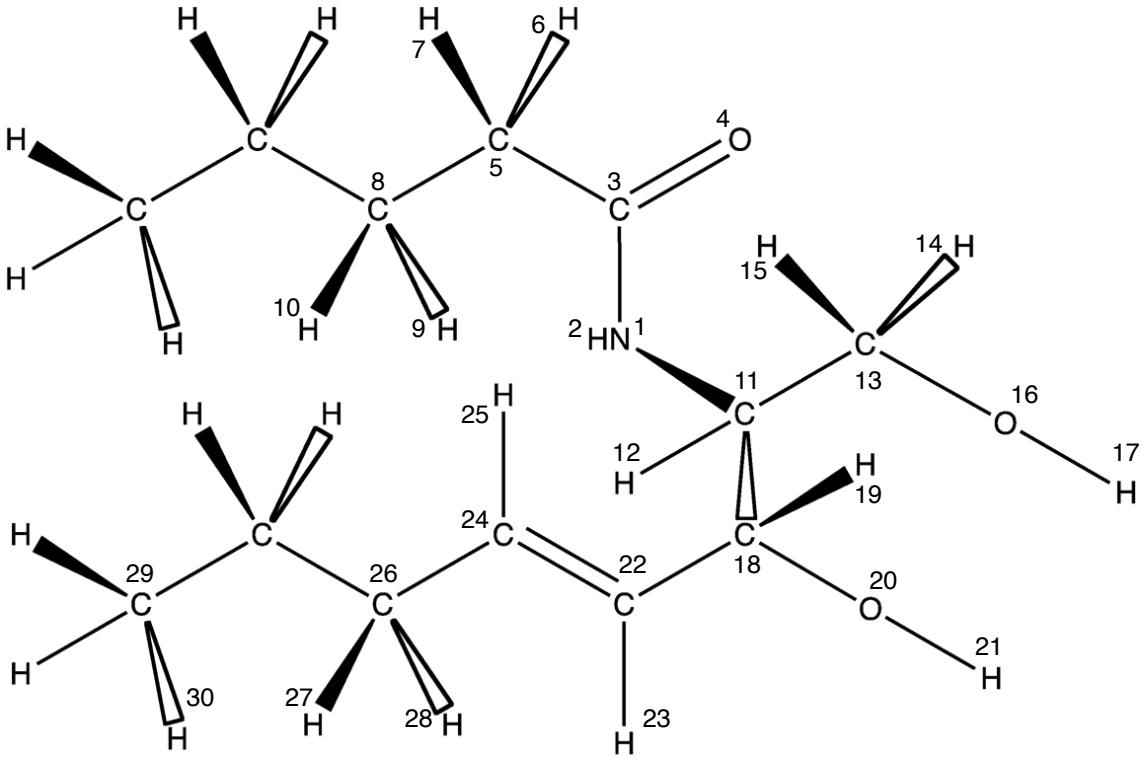

Figure S1. Structure of the truncated CER NS used in the *ab initio* calculation.

Table S2. Bond and angle parameters from *ab initio* calculation for the amide group. Atom index 1, 2, 3 and 4 are the nitrogen, hydrogen, carbon and oxygen in the amide group; atom index 11 is the carbon connected with the amide group to the phytosphingosine/sphingosine tail.

Amide bonded interactions	**BOND**	
	Force constant (kcal/mol/ Å^2)	**Equilibrium bond length (Å)**
N-H (1-2)	537.50	1.0108
N-C (1-3)	506.50	1.3659
N-C (1-11)	371.95	1.4668
C=O (3-4)	875.00	1.2302
C-C (3-5)	315.45	1.5269
	ANGLE	
	Force constant (kcal/mol/radian^2)	**Equilibrium angle (degree)**

N-C=O (1-3-4)	178.500	122.44
H-N-C (2-1-3)	78.875	119.61
H-N-C (2-1-11)	35.000	116.55
C-N-C (3-1-11)	108.500	123.36
N-C-C (1-3-5)	155.400	115.48
O-C-C (4-3-5)	203.100	118.09

Non-bonded interactions

The same eight random configurations, as used in the discussion above, were also used to determine the point charges of isolated CER NS and NP molecules. Single-point energy calculations were performed on the eight input data files and the partial charges subsequently obtained using the Mulliken population analysis. The results (shown for CER NS in Table S3) were averaged over all eight data files to obtain the partial charge for each atom. The structure and partial charges of the CER NS and NP molecules are shown in Figure 1 of the main document.

Table S3. Partial charge calculation results for truncated CER NS. Atom index is as that shown in Figure S1.

Index	Atom	Run 1	Run 2	Run 3	Run 4	Run 5	Run 6	Run 7	Run 8	Ave.	StdDev
1	N	-0.54	-0.55	-0.52	-0.53	-0.52	-0.52	-0.52	-0.53	-0.53	1.15E-02
2	H	0.26	0.26	0.27	0.25	0.26	0.26	0.26	0.26	0.26	3.94E-03
3	C	0.57	0.61	0.58	0.63	0.62	0.56	0.56	0.57	0.59	2.64E-02
4	O	-0.52	-0.52	-0.53	-0.52	-0.52	-0.54	-0.52	-0.53	-0.53	5.87E-03
5	C	-0.26	-0.26	-0.26	-0.28	-0.26	-0.25	-0.27	-0.28	-0.27	1.21E-02
6	H	0.13	0.12	0.13	0.14	0.13	0.12	0.13	0.13	0.13	5.72E-03
8	C	-0.17	-0.18	-0.17	-0.17	-0.17	-0.17	-0.18	-0.18	-0.18	4.51E-03
9	H	0.10	0.09	0.10	0.09	0.09	0.09	0.09	0.09	0.09	3.62E-03
11	C	0.05	0.05	0.05	0.03	0.02	0.03	-0.01	0.05	0.03	2.22E-02
12	H	0.11	0.13	0.11	0.12	0.11	0.12	0.11	0.13	0.12	1.30E-02
13	C	0.05	0.06	0.04	0.08	0.07	0.08	0.06	0.06	0.06	1.38E-02
14	H	0.08	0.09	0.12	0.10	0.11	0.11	0.10	0.11	0.10	1.31E-02
16	O	-0.56	-0.56	-0.55	-0.55	-0.55	-0.55	-0.56	-0.55	-0.55	5.34E-03
17	H	0.34	0.34	0.34	0.35	0.34	0.34	0.33	0.33	0.34	7.23E-03
18	C	0.13	0.13	0.13	0.15	0.16	0.18	0.17	0.14	0.15	1.86E-02
19	H	0.07	0.08	0.09	0.08	0.09	0.08	0.07	0.08	0.08	9.16E-03
20	O	-0.58	-0.57	-0.55	-0.54	-0.54	-0.56	-0.58	-0.56	-0.56	1.52E-02
21	H	0.34	0.34	0.34	0.34	0.34	0.34	0.34	0.35	0.34	8.39E-03

22	C	-0.10	-0.09	-0.09	-0.11	-0.09	-0.10	-0.07	-0.10	-0.09	9.95E-03
23	H	0.10	0.09	0.10	0.09	0.09	0.09	0.09	0.09	0.09	3.81E-03
26	C	-0.21	-0.21	-0.21	-0.20	-0.22	-0.23	-0.22	-0.22	-0.22	1.37E-02
27	H	0.10	0.10	0.11	0.12	0.11	0.11	0.10	0.10	0.11	5.65E-03
29	C	-0.32	-0.31	-0.30	-0.29	-0.32	-0.29	-0.30	-0.30	-0.30	1.03E-02
30	H	0.09	0.10	0.09	0.10	0.09	0.10	0.09	0.10	0.10	4.08E-03

Similar to the dihedral interactions, the van der Waals interactions for the amide group were taken from analogous parameters for atoms in a peptide bond as reported in the CHARMM protein force field[1]. All other head group dispersion parameters are available in the CHARMM lipid force field[2].

Structural metrics

Bilayer thickness

Several methods exist in the literature for measuring the bilayer thickness, (note, in all cases, *z* corresponds to the normal to the bilayer), including (1) measurement of the average *z* position of phosphates in each leaflet[7], (2) measurement of the distance between electron density peaks in *z* direction[8], and (3) calculation of the interface thickness which refers to the distance over which water density falls from 90% to 30% of bulk value [9]. In the systems studied here, since the highest *z* position for the head groups in the CERs varies between CER NS and NP, we determine the bilayer height by calculating the interface thickness. The bilayer thickness is extracted from the difference in *z*-values where water density drops to 1/*e* of its bulk value,[10] as illustrated in Figure S2.

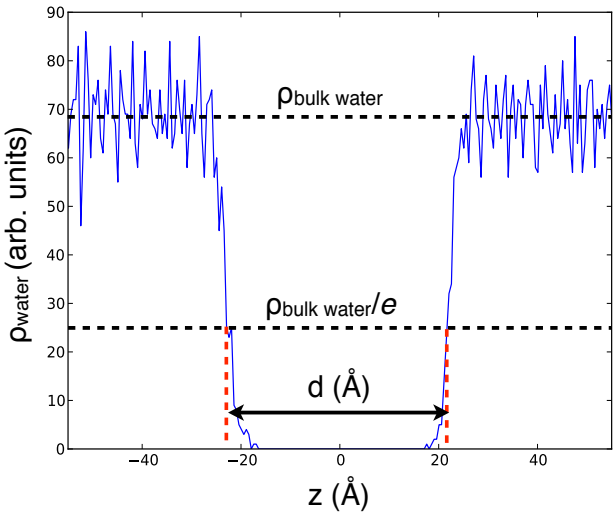

Figure S2. Measurement of bilayer thickness based on the water density profile.

Tail order parameter

To quantify the orientational order of the tail groups in a given leaflet, the nematic order parameter, S_2,[11] typically used for liquid crystalline systems, is calculated. First, the average direction of each lipid tail is quantified by calculating the moment of inertia tensor of the carbon backbone (or a subset of the carbon backbone in specific cases):

$$I_{\alpha\beta} = \sum_{i=1}^{N_l} m_i \sum \hat{\mathbf{r}}_i^2 \delta_{\alpha\beta} - \mathbf{r}_{i\alpha}\mathbf{r}_{i\beta} \quad , \qquad (1)$$

where $\hat{r}_i$ is the position vector of each particle i relative to the center of mass, and m_i is the mass of each particle i , $\delta_{\alpha\beta}$ is the Kronecker delta, N_l is the total number of particles in the tail segment, and α and β are looping variables that correspond to the coordinate axes (i.e., *x, y, z*). The characteristic vector describing the tail, $\hat{u}$, is the eigenvector associated with the smallest eigenvalue of the moment of inertia tensor. These vectors are used to construct the nematic tensor:

$$Q_{\alpha\beta} = \frac{1}{N_L}\sum_{i=1}^{N_L}\frac{3}{2}\mathbf{u}_{i\alpha}\,\mathbf{u}_{i\beta} - \frac{1}{2}\delta_{\alpha\beta} \quad , \tag{2}$$

where N_{L} is the total number lipid tails considered. The director of the system is the eigenvector associated with the largest eigenvalue of Q, and the nematic order parameter, S_2, corresponds to this largest eigenvalue of Q. S_2 can also be defined as,

$$S_2 = < \frac{3}{2}cos^2\theta - \frac{1}{2} > , \tag{3}$$

where θ is the angle between a tail's principal axis and the preferred direction (i.e., director) of the system and the angle brackets denote an ensemble average. A value of S_2 =1 indicates a perfect nematic crystal; in bilayers system, a fluid bilayer typically has a value of $S_2 < 0.8$, as determined by visual inspection. While in a free polymer system, a disordered fluid state would typically have a value of $S_2 < 0.3$, the interface between the lipids and water in the CER system induces increased nematic ordering, even for systems that are not very well ordered (hence, the larger value). Note, each leaflet in the bilayer is considered separated, as the orientation may differ, and the two values averaged.

Tilt angle

Tilt angle is defined as the deviation of the system director (described above) from the vector normal to the bilayer interface; in this case, the normal is assumed to be parallel with the z-axis of the coordinate frame.

Planar order parameter

To determine the degree of 2d crystalline ordering between the tails in the bilayer plane, a global order parameter is constructed using the superposition method, outlined in references.[12, 13] Briefly, the center of mass of each of the tails is calculated and projected onto the xy plane, where each leaflet is considered separately. Using these centers of mass, the nearest neighbor shell surrounding a given tail is determined. The collection of local clusters are then translated to a common origin, constructing what is commonly termed a bond-order diagram; systems with long range crystalline ordering will show correlations between nearest neighbor directions in this diagram. The bond order diagram is then converted to a scalar order parameter by taking the magnitude Fourier transform with a given frequency. In the case of hexagonal ordering, the 6^{th} frequency is used, which results in an order parameter from 0 to 1, with a maximum value of unity for ideal hexagonal crystalline packing. Note that this is different from taking the average of the first neighbor hexagonal ordering (i.e., the average value of the fourier transform of each cluster), since in that case, collective orientational ordering is not preserved during the calculation, and thus long range order cannot be assessed. The metric considered here, relyingh on superposition, enables the collective, long-range ordering to be determined.

References

1. MacKerell, A. D.; Bashford, D.; Bellott, M.; Dunbrack, R. L.; Evanseck, J. D.; Field, M. J.; Fischer, S.; Gao, J.; Guo, H.; Ha, S.; Joseph-McCarthy, D.; Kuchnir, L.; Kuczera, K.; Lau, F. T. K.; Mattos, C.; Michnick, S.; Ngo, T.; Nguyen, D. T.; Prodhom, B.; Reiher, W. E.; Roux, B.; Schlenkrich, M.; Smith, J. C.; Stote, R.; Straub, J.; Watanabe, M.; Wiorkiewicz-Kuczera, J.; Yin, D.; Karplus, M., All-atom empirical potential for molecular modeling and dynamics studies of proteins. *Journal of Physical Chemistry B* **1998,** *102* (18), 3586-3616.

2. Klauda, J. B.; Venable, R. M.; Freites, J. A.; O,ÄôConnor, J. W.; Tobias, D. J.; Mondragon-Ramirez, C.; Vorobyov, I.; MacKerell, A. D.; Pastor, R. W., Update of the CHARMM All-Atom Additive Force Field for Lipids: Validation on Six Lipid Types. *The Journal of Physical Chemistry B* **2010,** *114* (23), 7830-7843.
3. Pastor, R. W.; MacKerell, A. D., Development of the CHARMM Force Field for Lipids. *J. Phys. Chem. Lett.* **2011,** *2* (13), 1526-1532.
4. M. J. Frisch, G. W. T., H. B. Schlegel, G. E. Scuseria, M. A. Robb, J. R. Cheeseman, G. Scalmani, V. Barone, B. Mennucci, G. A. Petersson, H. Nakatsuji, M. Caricato, X. Li, H. P. Hratchian, A. F. Izmaylov, J. Bloino, G. Zheng, J. L. Sonnenberg, M. Hada, M. Ehara, K. Toyota, R. Fukuda, J. Hasegawa, M. Ishida, T. Nakajima, Y. Honda, O. Kitao, H. Nakai, T. Vreven, J. A. Montgomery, Jr., J. E. Peralta, F. Ogliaro, M. Bearpark, J. J. Heyd, E. Brothers, K. N. Kudin, V. N. Staroverov, R. Kobayashi, J. Normand, K. Raghavachari, A. Rendell, J. C. Burant, S. S. Iyengar, J. Tomasi, M. Cossi, N. Rega, J. M. Millam, M. Klene, J. E. Knox, J. B. Cross, V. Bakken, C. Adamo, J. Jaramillo, R. Gomperts, R. E. Stratmann, O. Yazyev, A. J. Austin, R. Cammi, C. Pomelli, J. W. Ochterski, R. L. Martin, K. Morokuma, V. G. Zakrzewski, G. A. Voth, P. Salvador, J. J. Dannenberg, S. Dapprich, A. D. Daniels, Ö. Farkas, J. B. Foresman, J. V. Ortiz, J. Cioslowski, and D. J. Fox, Gaussian 09, Revision A.1. In *Gaussian, Inc.*, Wallingford CT: 2009.
5. Avogadro: an open-source molecular builder and visualization tool. Version 1.03. http://avogadro.openmolecules.net/.
6. Hanwell, M.; Curtis, D.; Lonie, D.; Vandermeersch, T.; Zurek, E.; Hutchison, G., Avogadro: an advanced semantic chemical editor, visualization, and analysis platform. *Journal of Cheminformatics C7 - 17* **2012,** *4* (1), 1-17.
7. Reddy, A. S.; Warshaviak, D. T.; Chachisvilis, M., Effect of membrane tension on the physical properties of DOPC lipid bilayer membrane. *Biochimica et Biophysica Acta (BBA) - Biomembranes* **2012,** *1818* (9), 2271-2281.
8. Garidel, P., Structural organisation and phase behaviour of a stratum corneum lipid analogue: ceramide 3A. *Physical Chemistry Chemical Physics* **2006,** *8* (19), 2265-2275.
9. Notman, R.; den Otter, W. K.; Noro, M. G.; Briels, W. J.; Anwar, J., The Permeability Enhancing Mechanism of DMSO in Ceramide Bilayers Simulated by Molecular Dynamics. *Biophysical Journal* **2007,** *93* (6), 2056-2068.
10. Das, C.; Noro, M. G.; Olmsted, P. D., Simulation Studies of Stratum Corneum Lipid Mixtures. *Biophysical Journal* **2009,** *97* (7), 1941-1951.
11. Wilson, M. R., Determination of order parameters in realistic atom-based models of liquid crystal systems. *J. Mol. Liq.* **1996,** *68* (1), 23-31.
12. Keys, A. S.; Iacovella, C. R.; Glotzer, S. C., Characterizing complex particle morphologies through shape matching: Descriptors, applications, and algorithms. *Journal of Computational Physics* **2011,** *230* (17), 6438-6463.
13. Keys, A. S.; Iacovella, C. R.; Glotzer, S. C., Characterizing Structure Through Shape Matching and Applications to Self-Assembly. In *Annual Review of Condensed Matter Physics, Vol 2*, Langer, J. S., Ed. 2011; Vol. 2, pp 263-285.